Journal of Electroanalytical Chemistry 791 (2017) 117–123

Contents lists available at ScienceDirect

Journal of Electroanalytical Chemistry

journal homepage: www.elsevier.com/locate/jelechem

Electrochemical and spectroscopic investigation of a binary Ni-Co oxide active material deposited on graphene/polyvinyl alcohol composite substrate

Donatella Coviello [a], Michela Contursi [a], Rosanna Toniolo [b], Innocenzo G. Casella [a,*]

[a] Dipartimento di Scienze, Università degli Studi della Basilicata, Via dell'Ateneo Lucano 10, 85100 Potenza, Italy
[b] Dipartimento di Scienze Agro-Alimentari, Ambientali e Animali, Università degli Studi di Udine, Via Cotonificio, 108, 33100 Udine, Italy

ARTICLE INFO

Article history:
Received 9 November 2016
Received in revised form 11 January 2017
Accepted 28 February 2017
Available online 01 March 2017

Keywords:
Graphene oxide
PVA
Nickel
Cobalt
Electrochemical
SEM
XPS

ABSTRACT

A composite material based on Polyvinyl alcohol (PVA) and graphene oxide (GO) was used as electrode substrate for the Ni-Co electrodeposition in neutral chloride bath containing 1.5 mM $Ni(NO_3)_2$ and 4.5 mM $Co(NO_3)_2$. Ni-Co particles were cathodically deposited by voltage cycling between −0.5 V and 0.2 V vs. SCE (35 cycles). Voltammetric data show clearly an inhibition phenomenon of nickel oxide deposition upon increasing $[Co^{2+}]$ in the electroplating baths. Nevertheless, the presence of electrodeposited Co oxide species induces beneficial effects on the redox electrochemical behavior of the GC/PVA/GO/Ni-Co electrode in alkaline medium (0.1 M NaOH). The resulting electrode shows, a unique and reversible symmetrical cathanodic wave centered at about 0.3 V vs SCE. The SEM analysis shows the graphene oxide disposed as platelets in a agglomerate distribution randomly oriented within the PVA matrix. The electrodeposition process of Ni-Co species proceeds preferentially on the GO platelets surfaces. After the charge/discharge process in alkaline medium, the Ni-Co deposit shows a globular inhomogeneous distribution with an average diameter comprised between 50 nm and 300 nm. The XPS characterization of the electrodeposited Ni-Co catalyst reveals a surface chemical composition of about $Ni_{16}Co_{84}$, confirming an "anomalous" co-deposition process of the metals on the PVA/GO electrode substrate.

1. Introduction

Chemically modified electrodes (CMEs), based on the use of innovative materials, show interesting physicochemical and electrochemical properties [1]. In particular, surfaces of traditional electrodes modified with deposited films of oxides and oxyhydroxides of various transition metals have attracted a great deal of interest in view of their potential applications in many scientific and technological fields such as: photoelectrochemistry [1–4], corrosion suppression [5,6], primary and secondary energy storage devices [7–10], electrochromic devices [11,12], electrocatalysis and electrochemical sensors etc., [13–17].

Main attempts have been made to use large numbers of transition metal oxides, including both bulk and nanostructures-based electrode materials, such as NiO_x, CuO_x, MnO_2, RuO_2, CoO_x, IrO_x, etc. Often, mixed catalyst oxides are of better electrochemical properties and stability than the monometallic ones. For example, the electrocatalytic enhancement of Pt alloys with transition metals has been attributed to the change of d-electron density in platinum atoms due to alloy formation [18–20]. Among these electrochemical materials, Pt-Ni nanoparticles are useful characterized as suitable and attractive materials as cathode or anode components in fuel cell applications or electrocatalyst materials [14,20,21,22]. Likewise, several studies have found that the presence of certain metal oxide species such as cobalt, zinc, cadmium, etc. can affect the electrocatalytical behavior of the nickel electrocatalyst. Thus, Ni-Co binary oxide layer were fabricated and characterized as efficient electrocatalysts for oxidation of small organic molecules and/or oxygen evolution reactions [13,17,23–25]. In addition, binary $Ni_{1-x}Co_x$ layered double hydroxides were synthesized, characterized and usefully proposed as innovative supercapacitor electrode materials, showing superior rate capability, energy efficiency and considerable specific capacitance [9,25–30]. In this respect, cathodic electrochemical codeposition of nickel and cobalt species allows the formation of open porous three-dimensional dendritic structures, useful for redox supercapacitors and heterogeneous catalysts [25–27,31]. On the other hand, some Ni-Co oxides such as $NiCo_2O_4$ species, thanks to their spinel structure, show a conductivity above two order of magnitude higher than individual transition metal oxides [31]. A substantial increase in electrical conductivity of the active electrode material improves the reversible faradic character of electrode redox couples. Despite the potential electrochemical properties of the combined mixed oxide systems, generally these

* Corresponding author.
E-mail addresses: rosanna.toniolo@uniud.it (R. Toniolo), innocenzo.casella@unibas.it (I.G. Casella).

http://dx.doi.org/10.1016/j.jelechem.2017.02.048
1572-6657/

performance decline dramatically with the increasing loading mass of the active electrode material on the electrode surface. To tackle these problems, one of the key strategies is to develop composite materials, where the active catalyst can be efficiently dispersed into nanostructured conductive substrates in order to improve the surface exposure of the active electrode particles.

Graphene and nanotubes materials (CNTs) have captured a great attention and interest in the scientific contexts due to their useful electrical, chemical and mechanical properties. In particular, the graphene, a two-dimensional (2D) nanomaterial with a single sheet of carbon atoms packed in a hexagonal lattice, has recently attracted attention due to its unique chemical and physical properties. In this respect, graphene based composites with metal oxides have been successfully proposed in several technological applications [32–35]. Recently, 3D interconnected graphene nanostructures were characterized and proposed as innovative substrate electrode materials [34,35], exhibiting an open-pore honeycomb structure, where this 3D graphene structure shows exceptional large void volume, high surface area and good electrical conductivity. Graphene oxide (GO), one of the most important derivatives of graphene is characterized by a layered structure with oxygen functionalities groups bearing on the basal planes and edges, and thanks to its versatile chemical and physical properties make it attractive for fundamental research as well as in technological applications of interest [36]. In this respect, electrodeposited reduced-graphene oxide (rGO) containing Co species were successful characterized for charge storage applications, showing a remarkable enhancement in the electrochemical response pointing to a synergistic effect between the graphene structure and deposited Co oxide particles [37,38].

Simple metal adsorption on the defect sites of the graphene or CNTs surfaces, leads to poor dispersion degree of the catalyst and generally a bad stability of the electrodic active materials. Thus, effective dispersion of carbonaceous materials such as nanotubes or graphene species in polymers is of significant interest as it promises to impart improved mechanical barrier properties and/or electrical/capacitance character. In order to obtain stable composite electrode configuration, often the metal catalysts species and nanostructured electrode substrate must be linked together via covalent bonds and/or dispersed in stable polymer matrices, such as nafion, polyaniline, polypyrroles, etc. [39–41]. Often, the polymer matrix acts as perm-selective barrier useful to prevent poisoning phenomenon of the active redox catalysts entrapped within composite electrode materials. Polyvinyl alcohol (PVA) is a water soluble, biologically compatible, non-toxic and readily available low-cost synthetic polymer of great interest in many biomedical applications [42]. In addition, studies on PVA-based systems have shown that they exhibit interesting electrical properties useful for potential applications in fuel cells and double-layer capacitors [43,44].

In this study, we have extended the idea of exploring the electrochemical potentialities of a composite electrode material based on the combined GO and PVA film containing electrodeposited oxide nanoparticles of nickel and cobalt species (Ni-Co). In this respect, strong hydrogen bonds between GO and PVA matrix were well observed and considered responsible of significant enhancements in mechanical and thermal stability of the PVA/GO composite [43–45]. Nevertheless, on the basis of our knowledge there are no studies regarding the electrochemical and spectroscopic characterization of the PVA/GO composite as substrate electrode containing these metal catalysts (Ni-Co). As consequence, in this study the composite electrode material, defined as GC/PVA/GO/Ni-Co, was characterized by electrochemical, X-ray photoelectron spectroscopy (XPS) and scanning electron microscopy (SEM) techniques. The electrochemical properties of the composite electrode were investigated in alkaline medium (0.1 M NaOH).

2. Experimental

2.1. Reagents

The stock solutions were prepared by using ultrapure water supplied by a Millipore Direct-Q UV unit (Bedford, MA, USA). Polyvinyl alcohol (Mw:130.000, 99% hydrolyzed), graphene oxide (powder, 15–20 sheets, 4–10% edge-oxidized), $Ni(NO_3)_2$ hexahydrate (≥98.5%), $Co(NO_3)_2$ hexahydrate (≥99.5%), NaOH pellets (≥98%), were purchased from Sigma-Aldrich (Germany). GO (20 mg) were dispersed in 5 mL H_2O and sonicated for 2 h at room temperature. Similarly, 20 mg PVA were dissolved in 5 mL H_2O and sonicated for 2 h at 80 °C. Fresh aqueous emulsion of GO/PVA having mass ratio (w/w): 5, 10, 20, 30 and 40, were prepared before use by mixing appropriate amount of PVA solution (4 mg/mL) and GO emulsion (4 mg/mL).

The effective good dispersion of GO is maintained by the electrostatic repulsion of carboxylate groups present on the structure, showing these materials a typical zeta potential of about - 0.64 mV when they are dispersed in aqueous solutions [46,47].

2.2. Apparatus

The voltammetric experiments were performed with an Autolab PGSTAT 30 Potentiostat/Galvanostat (Eco Chemie, Utrecht, The Netherlands) and the data were acquired using an Autolab GPES software package version 4.9. Cyclic voltammetry (CV) was done in a three-electrode cell using the GC/PVA/GO/Ni-Co as working electrode, a SCE reference electrode and a platinum foil counter electrode (Amel, Italy). The glassy carbon (GC) substrates (3 mm diameter), used in all experiments, were also purchased from Amel (Milan, Italy). All current densities in this paper were quoted in terms of mA cm^{-2} of apparent geometric area of substrate electrode. The experiments were carried out at room temperature (20 ± 2 °C).

The morphological analysis of the various electrode materials was performed with an environmental scanning electron microscope (SEM) Philips-FEI ESEM XL 30, endowed with a lanthanum hexaboride (LaB_6) source. The samples were put on a stub with a bi-adhesive film to ensure sample adhesion and the vacuum pressure in the chamber was maintained below 7×10^{-8} bar.

X-ray photoelectron spectra were collected using a Leybold LH X1 spectrometer using unmonochromatized Al Kα radiation (1486.6 eV). The source was operated at 15 kV and 20 mA. The binding energy (BE) scale was calibrated with respect to the Cu $2p_{3/2}$ (932.7 eV, with a full-width at half-maximum (FWHM) of 1.6 eV) and Au $4f_{7/2}$ (84.0 eV with a FWHM of 1.3 eV) signals. Spectra were recorded only after the wide scan showed that no features arise from the copper tape and from the sample rod. Wide and detailed spectra were collected in fixed analyzer transmission (FAT) mode with a pass energy of 50 eV and a channel width of 1.0 and 0.1 eV, respectively. The vacuum in the analysis chamber was always better than 5×10^{-9} mbar.

The kinetic energy axis origin in all spectra was not corrected for surface charging, but peak positions in the text are corrected by referring to the C 1s peak after setting its BE to 284.6 eV. Satellites and a nonlinear Shirley background were subtracted from the spectrum before curve fitting analysis. Elemental surface stoichiometries were obtained from peak area ratios corrected by appropriate sensitivity. Gaussian/Lorenzian sum functions were used to fit Ni $2p_{3/2}$, Co $2p_{3/2}$, O 1s and C 1s peaks line-shapes.

2.3. Electrode preparation

Before modification, the glassy carbon surfaces were polished with 0.05 μm α-alumina suspension on a micro-cloth polishing pad, washed with HCl (15%) and finally with ultrapure water to remove traces of surface impurities. The polished glassy carbon electrodes were modified with 10 μL of the casting GO/PVA emulsion. Unless otherwise specified,

casting GO/PVA emulsion having a mass ratio of 5 was used to modify the electrode surface. The modified electrodes were dried in an oven at about 50 °C for 20 min and then rinsed with ultrapure water. The resulting electrodes were cycled between −0.5 V and 0.2 V vs. SCE (35 cycles) in a not de-aerated 5.8 mM KCl solution containing 1.5 mM $Ni(NO_3)_2$ and 4.5 mM $Co(NO_3)_2$. The prepared electrodes were defined as GC/PVA/GO/Ni-Co.

The apparent active surface loading (Γ, nmol) of electrodeposited metal oxides, expressed as Ni metal species, was evaluated under cyclic voltammetry (CV) by integrating the anodic wave I_a, corresponding to the nominal redox transition of the Ni(II)/Ni(III) species. Assuming that under wave I_a is operative only the Ni^{2+}/Ni^{3+} redox transition couple and considering that all Ni surface particles are electroactive on the voltammetric time scale considered, a nominal surface loading of Ni species (Γ) comprised between 1.6 nmol and 1.9 nmol, was obtained.

3. Results and discussion

3.1. Preparation and electrochemical characterization

The metal deposition process was performed by cycling the potential between −0.5 V and 0.2 V vs. SCE (35 cycles) in a not de-aerated 5.8 mM KCl solution containing 1.5 mM $Ni(NO_3)_2$ and/or 4.5 mM $Co(NO_3)_2$. The presence of two distinct solid solutions during the cathodic deposition, one of cobalt and another of nickel, in the electrodeposited materials having an atomic concentration of the elements of $Co_{70}Ni_{30}$, was already observed by XRD studies [26,27]. In addition, the solubility and the mutual solubility of the metals decreases with increasing Co content in the deposit. Thus, the formation of Ni–Co alloys during the cathodic electrodeposition, can be reasonably excluded (vide infra). Fig. 1 shows a comparison between the voltammogram profiles of GC/PVA/GO/Ni and GC/PVA/GO/Co modified electrodes obtained in 0.1 M NaOH. The GC/PVA/GO/Ni modified electrode shows the typical Ni(II)/Ni(III) redox transition, including a well defined irreversible cathanodic wave, indicated as I_a/I_c and centered between 0.3 V and 0.5 V vs. SCE. The complexes redox processes of nickel species involve, in agreement with the literature [48,49], anhydrous β-$Ni(OH)_2$, hydrated α-$Ni(OH)_2$, oxidized phases β-NiOOH and/or γ-NiOOH. These species can coexist during continuous cycling polarization in alkaline medium [7,50,51]. The voltammogram profile of the GC/PVA/GO/Co shows a large oxidation wave located at potentials higher than 0.3 V due to Co(II)/Co(III) and Co(III)/Co(IV) redox transitions; this electrochemical wave can be attributed to the simultaneous conversion of various cobalt species such as $Co(OH)_2$, Co_2O_3, Co_3O_4, CoOOH, CoO_2, etc. [52,53]. The observed broadness of the redox transition and its relevant electrochemical properties could be connected with roughness and porosity of the cobalt active sites, involved allotropic phases and specific

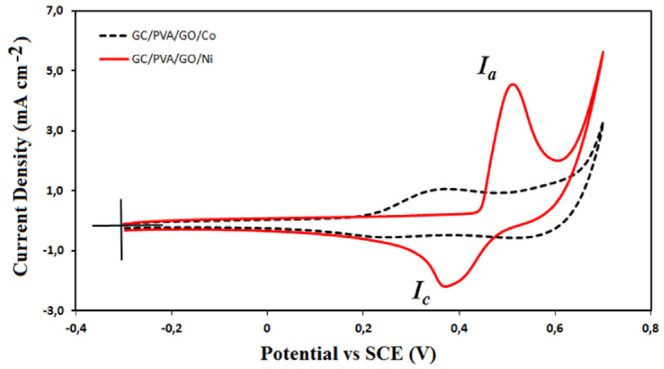

Fig. 1. Cyclic voltammograms (50 mV s^{-1}) of GC/PVA/GO/Ni (solid curve) and GC/PVA/GO/Co (dashed curve) modified electrodes obtained in 0.1 M NaOH. The metal deposition was obtained by cycling the potential between −0.5 V and 0.2 V vs. SCE (35 cycles) in a not de-aerated 5.8 mM KCl solution containing 1.5 mM $Ni(NO_3)_2$, or 4.5 mM $Co(NO_3)_2$.

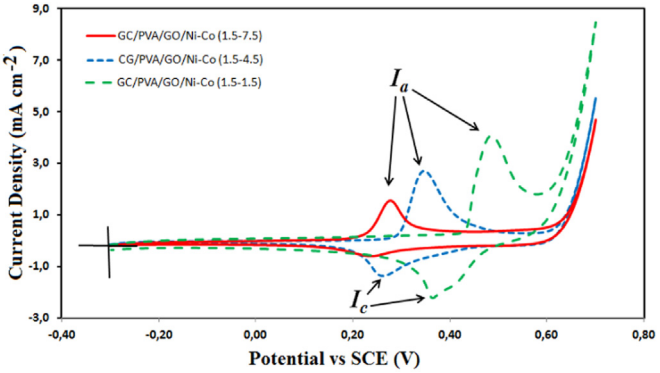

Fig. 2. Cyclic voltammograms (50 mV s^{-1}) of GC/PVA/GO/Ni-Co modified electrodes obtained in 0.1 M NaOH. The Ni-Co metal deposition was obtained by cycling the potential between - 0.5 V and 0.2 V vs. SCE (35 cycles) in a not de-aerated 5.8 mM KCl solution containing various concentration ratios of $Ni(NO_3)_2$ and $Co(NO_3)_2$.

electrode substrate. In fact, the specific behavior of these oxides is strictly related to the actual chemical and physical status of the electrode surface, composition of the electrolytic solution, polarization time and applied potentials [52–55]. The Fig. 2 shows the voltammograms of the GC/PVA/GO/Ni-Co modified electrode in alkaline medium. As can be seen in figure, the I_a/I_c wave is shifted to lower potentials in presence of increased Co oxide species in the Ni-Co deposits. The relevant voltammograms exhibit a unique I_a/I_c well distinct redox system rather than two individually cathanodic contributes. The voltammogram profiles of the GC/PVA/GO/Ni-Co system appear quite similar to those reported for other nano and mesoporous $Ni_xCo_y(OH)_z$ binary oxides obtained in alkaline medium [13,17,23–25]. This observed potential shifting toward cathodic potentials is indeed a great feature taking into account the development of electrochemical devices, where the relevant electroactivity can be explicated in a potential region which there is no oxygen evolution contributes (i.e., between 0.3 V and 0.55 V vs SCE). The effect of the $[Ni^{2+}]:[Co^{2+}]$ concentration ratio in the plating bath solution, on the voltammogram profiles of the GC/PVA/GO/Ni-Co system, is summarized in Table 1. As it can be seen, under voltammetric conditions, the following interesting findings can be drawn:

i) the apparent formal potential of the redox system, expressed as $(E_{pa} + E_{pc}) / 2$, shifts gradually toward more cathodic values with increasing $[Co^{2+}]$ content in the plating bath, reaching a minimum potential value of 0.25 V at the $[Ni^{2+}]:[Co^{2+}]$ concentration ratio of 0.3;
ii) the ΔE_p parameter, expressed as $(E_{pa} - E_{pc})$, decreases significantly on decreasing $[Ni^{2+}]:[Co^{2+}]$ concentration ratio. As can be seen, the ΔE_p decreases from 120 mV to 30 mV as on passing the $[Ni^{2+}]:[Co^{2+}]$ concentration ratio of ∞ to 0.2;
iii) the active surface loading (Γ, nmol) of electrodeposited oxides, decreases markedly on increasing $[Co^{2+}]$ in the plating bath

Table 1
Effects of the $[Ni^{2+}]:[Co^{2+}]$ contained in the plating bath solution on the voltammogram profile of the GC/PVA/GO/Ni-Co electrode.

$[Ni^{2+}]:[Co^{2+}]$	R	ΔE_p (mV)	$(E_{pa} + E_{pc}) / 2$ (mV; SCE)	Γ (nmol)
1.5:0.0	∞	120	420	2.3
1.5:1.5	1	80	300	2.1
1.5:4.5	0.3	50	250	1.7
1.5:7.5	0.2	30	250	0.95

The Ni-Co deposition was obtained by cycling the potential between −0.5 V and 0.2 V vs. SCE (35 cycles) in a not de-aerated 5.8 mM KCl solution containing $Ni(NO_3)_2$ and $Co(NO_3)_2$ at various concentration ratios (R).
ΔE_p represents the peak potential differences between E_{pa} and E_{pc} ($E_{pa} - E_{pc}$);
Γ represents the apparent active surface loading (nmol) of electrodeposited metal oxides, expressed as Ni metal species. It was evaluated in 0.1 M NaOH by cyclic voltammetry (50 mV s^{-1}) by integrating the anodic wave I_a.

solution. In fact, the surface loading of the deposited oxides on the GC/PVA/GO/Ni-Co electrode increases from 0.96 nmol to 2.3 nmol (i.e., about 140%) when the $[Ni^{2+}]$:$[Co^{2+}]$ concentration ratio was increased from 0.2 to ∞ (i.e., free Co^{2+} plating bath solution);

iv) the presence of Co species increases the over potential of the oxygen evolution reaction (OER) (see Fig. 2), thus the electrochemical utilization of the GC/PVA/GO/Ni-Co electrode is improved up to about 0.55–0.60 V vs SCE without to observe a sensible oxygen discharge process.

The summarized results reported in Table 1 show that upon increasing $[Co^{2+}]$ in the electroplating bath solution, a clear inhibition of nickel oxide deposition was observed. The simultaneous electrodeposition of Ni-Co species occurs often in an anomalous manner [56–58], where the thermodynamically less noble metal deposits preferentially rather than the more noble metallic ions. In this study, an anomalous co-deposition of Ni-Co species on the GC/PVA/GO substrate was observed (vide infra). Although many models have been proposed, the mechanism of the anomalous co-deposition of Ni-Co species is not fully understood and several partial interpretations have been proposed [56–58]. In agreement with the literature, the schematic mechanism for the cathodic electrodeposition of Ni-Co metals involves two consecutive one-electron charge transfers, with the active participation of ligand species and formation on the electrode surface of adsorbed complexes:

$$M^{2+} + X^{-} \Longleftrightarrow MX^{+} \quad (1)$$

$$MX^{+} + e^{-} \Longleftrightarrow MX_{(ads)} \quad (2)$$

$$MX_{(ads)} + e^{-} \Longleftrightarrow M + X^{-} \quad (3)$$

where M^{2+} indicates both Co^{2+} or Ni^{2+} metal ions, while the X^{-} has been variously assumed to be OH^{-}, Cl^{-}, etc. or hydrogen atoms (H_{ads}). The adsorption ability of $CoOH^{+}$ on the electrode substrate and/or other $CoX_{(ads)}$ species can inhibit the subsequent adsorption/reduction of nickel complex species such as $NiOH^{+}$, inducing the anomalous co-deposition phenomena [57,58].

Although the inclusion of Co species in Ni oxyhydroxide particles is widely investigated and proposed in order to improve the electrochemical reversibility of the Ni(II)/Ni(III) redox transition and increase the oxygen evolution potential [13,17,24,25,59–63], the exact mechanism regarding the possible electrochemical interaction between nickel and cobalt species is still less understood. Based on the experimental data (vide infra) and in agreement with several literature data [59–64], the beneficial effects of cobalt oxides on the electrochemical behavior of the GC/PVA/GO/Ni-Co system can be interpreted considering a synergistic combination between the following factors:

a) The GC/PVA/GO/Ni-Co electrode shows a unique well symmetrical cathanodic wave, while in absence of Co species, the electrode shows two overlapped cathodic waves (see Fig. 1) confirming that more than one phase of Ni oxide is formed during the charge/discharge process. Thus, the cobalt addition can alter the basic allotropic phases of the Ni(II)/Ni(III) oxides, avoiding the development of inactive phases (i.e., γ-NiOOH structure). This factor can improve significantly the electrical and mechanical properties of the nickel oxides during the charge/discharge processes. In this respect, we have demonstrated that the use of Cu oxyhydroxide additive imparts an extensive stabilization of the active α/β crystallographic forms of the nickel hydroxide structures [65].

b) The formation of some Co species, having a good conducting character, can decrease the overall electrical resistance of the deposit and hence increase the electrochemical performance of the Ni-Co redox system.

At this time, we are unable to define to real contribution of each considered previous factor or discriminate between electron or ion conductivity about the increased electrochemical reversibility of the GC/PVA/GO/Ni-Co electrode, nevertheless the cobalt codeposited species introduce interesting features (i.e., improved electrochemical reversibility), very useful in fundamental and applied sciences.

In order to investigate the effects of the GO, as surface modifying substrate, on the kinetics of the nickel electrodeposition process, we have compared the electrochemical performance of the modified electrodes with and without the GO platelets (i.e., GC/PVA/GO/Ni vs GC/PVA/Ni). It is interesting to observe that, the active surface loading (Γ, nmol) of electrodeposited oxides, evaluated by integrating the anodic wave I_a, is significantly affected by the presence of the GO on the electrode surface. In fact, the metal oxide surface concentration (Γ) changes from ca 0.63 nmol (i.e., 60 μC) to 2.5 nmol (i.e., 0.24 mC) if on the GC electrode are deposited 10 μL of the casting GO/PVA emulsion (mass ratio of 5). Thus, an increase of about 300% of the Γ in presence of structured GO particles, was observed. The GO platelets can induce an increase in the surface roughness factor with a favorable inside three-dimensional distribution of the catalyst on the surface electrode; consequentially a marked increases of the electrochemical redox efficiency of the Ni-Co catalyst is observed.

3.2. Surface characterization: SEM analysis

Scanning electron microscopy was employed in order to investigate the morphological structure of the GC/PVA/GO/Ni-Co electrode, before and after electrochemical treatment in alkaline solution. Fig. 3 shows a representative surface morphology of the GC/PVA/GO electrode, obtained by casting 10 μL of the GO/PVA emulsion having a mass ratio of 5. The image shows that the graphene oxide particles appear in an agglomerate distribution and are randomly oriented within the PVA matrix forming interconnecting structures. The SEM analysis reveals that the GO particles are present in the composite electrode material as single, exfoliated sheets or as multi-layered platelets, indicating clearly a disorder three-dimensional (3D) distribution of the agglomerated nanoplatelets of GO on the entire electrode surface. The practical absence of charging during SEM analysis suggests that the network of graphene-based sheets are sufficiently electrically conductive. Fig. 4

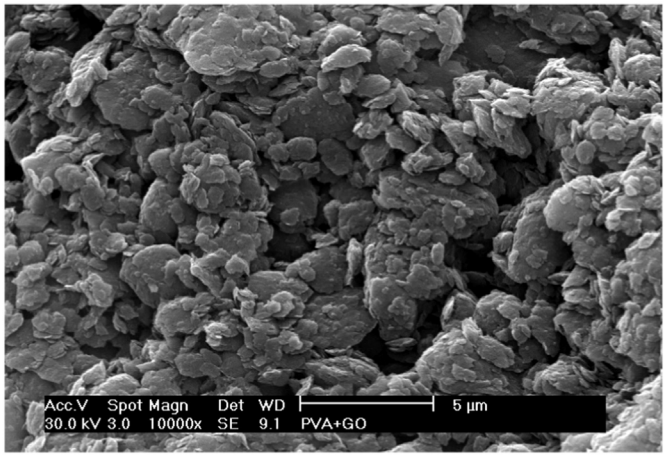

Fig. 3. SEM picture of the GC/PVA/GO substrate electrode obtained by casting 10 μL GO/PVA emulsion having a mass ratio of 5 (i.e., 20 μL PVA (4 mg/mL) + 100 μL GO (4 mg/mL)). The modified electrode was dried in an oven at 50 °C for 20 min and rinsed with ultrapure water.

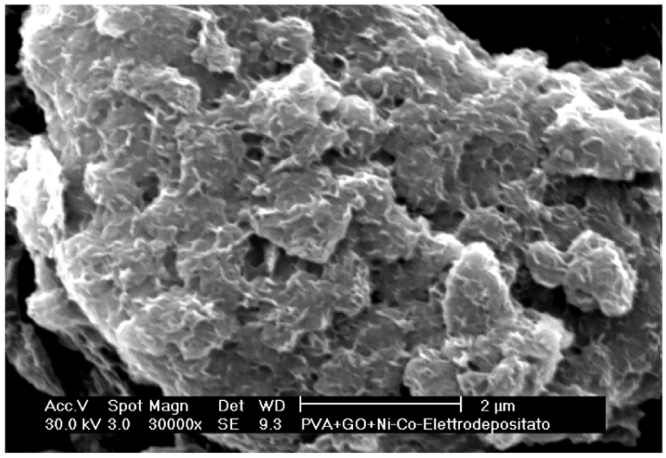

Fig. 4. SEM picture of the GC/PVA/GO/Ni-Co electrode obtained by cycling potentials (35 cycles) in 5.8 mM KCl solution containing 1.5 mM $Ni(NO_3)_2$ and 4.5 mM $Co(NO_3)_2$. Other experimental conditions as in Fig. 3.

shows a detailed scanning electron micrograph of the GC/PVA/GO/Ni-Co electrode without any electrochemical treatment. It can be seen that, the electrodeposition process of Ni-Co species proceeds preferentially on the GO platelets substrate and the relevant microstructures show an average thickness value comprised between 20 and 40 nm. A similar physical distribution of Ni-Co hydroxide layers was obtained onto stainless steel by potentiostatic deposition method under cathodic conditions [66]. Fig. 5 shows a typical image of GC/PVA/GO/Ni-Co electrode after a prolonged charge/discharge treatment by potential cycling in 0.1 M NaOH (i.e., 200 scans of potential scans between −0.1 and 0.7 V vs. SCE). As can be seen, the electrochemical treatment of the electrode strongly influence the morphology of the electrodeposited Ni-Co species. A detailed analysis of the SEM image reveals that the Ni-Co deposit shows a globular inhomogeneous distribution of the particles well dispersed on the GO platelets. The small globular particles, having irregular forms with an average diameter comprised between 50 nm and 300 nm, appear isolated or dispersed as twinned or rarely multiply twinned complexes islands. The surface morphology of the electrodeposited Ni-Co remains sufficiently stable even after additional prolonged charge/discharge treatments in alkaline medium, in fact (see comparison between Figs. 4 and 5) the morphology of the PVA/GO substrate material remains practically unchanged during the entire electrochemical treatment of the electrode in alkaline medium, showing a considerable chemical and physical stability.

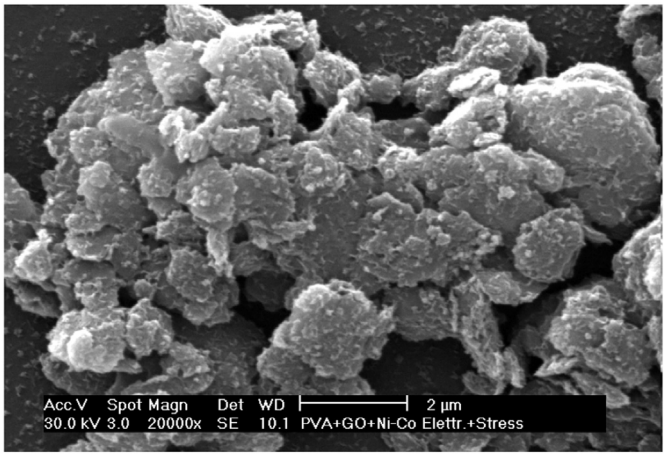

Fig. 5. SEM picture of the GC/PVA/GO/Ni-Co electrode after electrochemical treatment by potential cycling in 0.1 M NaOH (i.e., 200 scans of potential between −0.1 and 0.7 V vs. SCE). Other experimental conditions as in Fig. 4.

3.3. Surface characterization: XPS analysis

In order to investigate the surface chemical composition of the electrode material, we analyze and compare the detailed spectra of the C 1s, O 1s, Ni $2p_{3/2}$, and Co $2p_{3/2}$ regions of the GC/PVA/GO, GC/PVA/GO/Ni and GC/PVA/GO/Ni-Co surfaces. Typical C 1s, Ni $2p_{3/2}$, and Co $2p_{3/2}$ XP spectra of the electrochemical treated GC/PVA/GO/Ni-Co are shown in Figs. 6–8. Data acquisition and analysis of the detailed regions were performed by in-house data processing program, and the sensitivity factors used in quantifying spectra have previously specified [67,68]. The C 1s (Fig. 6) signal exhibits the graphitic peak and a significant asymmetric tailing toward higher binding energy (BE) values. According to literature information, a small chemical shift can be observed between aromatics/graphite and aliphatic hydrocarbons, and each carboxylic group on the aromatic ring shifts the C 1s peak by about 0.5 eV toward higher BE values [68]. The tail arises mainly from oxygen-containing functional groups such as alcohol (C-OH), ketone (C═O), carboxylic species (COOH), etc. [66]. As can be seen, the C 1s region shows three or four contributes at 284.6 eV ± 0.2 (C_1), 286.3 eV ± 0.2 (C_2), 287.8 eV ± 0.2 (C_3), and 289.1 eV ± 0.2 (C_4), which can be attributed to various kinds of carbon atoms including mainly the C-C/C-H, C-OH, C═O and COOH species [67,68]. At this time, we are unable to distinguish to real peak contribution of the C 1s signal arising from GC surface, GO and PVA matrix. Nevertheless, we are interested at this time to consider only the areas of the oxygen-containing functional groups. The Fig. 7 shows the XP spectra of the Ni $2p_{3/2}$ detailed region of the GC/PVA/GO/Ni-Co electrode. The Ni $2p_{3/2}$ spectrum shows a typical structure with intense satellite signals at high BE adjacent to the main peak, which may be ascribed to a multielectron excitation (shake-up peaks). The main Ni $2p_{3/2}$ peak could be deconvoluted generally into two components at about 856.2 ± 0.3 eV and 858.8 ± 0.3 eV, assigned to Ni(II) and Ni(III) oxyhydroxide species, respectively, in agreement with the literature data [49,67–71]. The full width half maximum (FWHM) range used (between 1.1 eV and 1.3 eV) was chosen on the curve fitting of previous studies [67–71]. As can be seen, the XPS signal is characterized by sufficiently high-intensity shake up satellites at higher BE than the main $2p_{3/2}$ signals, confirming the presence of oxidized nickel species [67,71]. The Fig. 8 shows the Co $2p_{3/2}$ XP signal of the GC/PVA/GO/Ni-Co electrode. In general, the Co 2 p XPS spectra consists of two main signals relevant at Co $2p_{3/2}$ and Co $2p_{1/2}$ having the spin-orbit splitting of about 16 eV. Similarly at the Ni $2p_{3/2}$ signal, the Co $2p_{3/2}$ shows a complex structure composed of a main signal with shake-up peaks at high binding energy, with energy separation of about 7.0 eV. The main Co $2p_{3/2}$ peak could be deconvoluted into two components at about 781.0 ± 0.5 eV and 783.0 ± 0.5 eV, which on the basis of

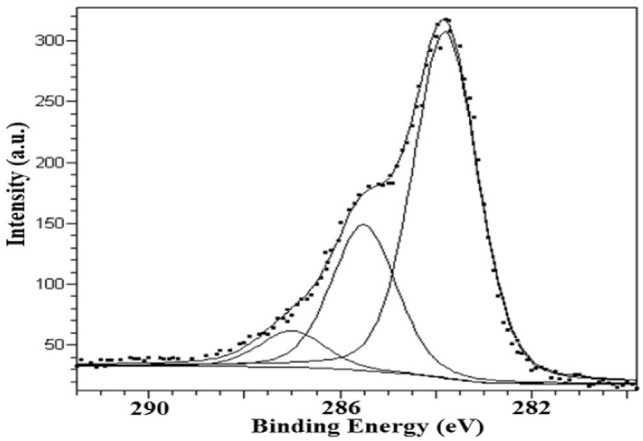

Fig. 6. XPS detailed C 1s region of the GC/PVA/GO/Ni-Co electrode. Conditions as in Fig. 4.

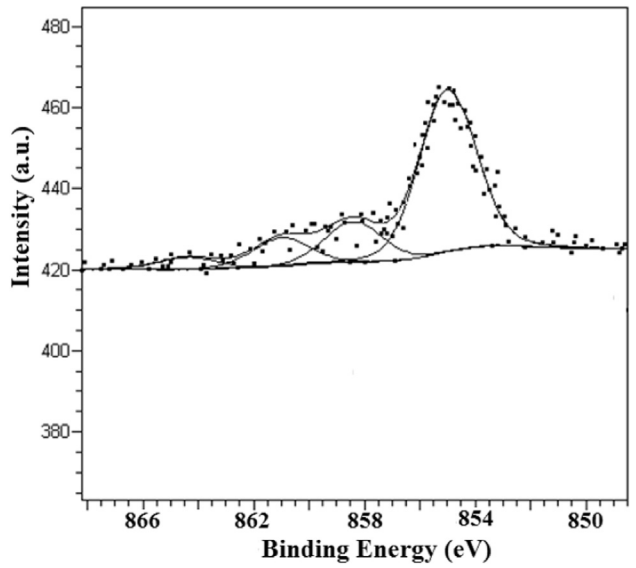

Fig. 7. XPS detailed Ni $2p_{3/2}$ region of the GC/PVA/GO/Ni-Co electrode. Conditions as in Fig. 4.

their BEs were assigned to Co(II) and Co(III) oxide and/or hydroxide species, respectively [67,72,73]. The presence of the complex satellites (shake-up peaks) at higher BE than the main $2p_{3/2}$ signals, confirms the practical absence of Co species at zero oxidation state [72,73]. Considering that very similar values of the BEs are known for most Co species, the presence of several stabilized mixed oxides such as Co_2O_3, Co_3O_4, CoO_2, etc., cannot be excluded. Nevertheless, in this study we consider the total area of the Co $2p_{3/2}$ signal, without to define the exact atomic ratio between the various possible Co oxide species. The curve fitting of the O 1s signal (not shown) indicates that there are usually up to three component peaks with binding energy comprised between 529 and 534 eV. The exact assignment of the O 1s contributes is complex and ambiguous owing to uncertainty in the *BE* values of the various oxygen species. However, in this study, we consider, in view of the comparison between the different surfaces, only the total area of the O 1s signal (O $1s_{tot}$). Consequently, the exact assignment of the specific peaks under the O 1s signal in this context, is not essential.

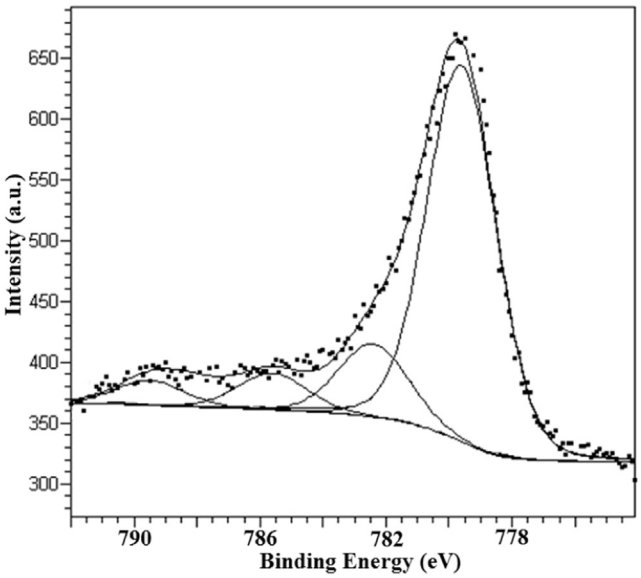

Fig. 8. XPS detailed Co $2p_{3/2}$ region of the GC/PVA/GO/Ni-Co electrode. Conditions as in Fig. 4.

In order to obtain useful information regarding the metal oxide composition ($(Ni\text{-}Co)_xO_y$) of the active material, the atomic ratios R(O/M) expressed as:

$R(O/M) = (O\ 1s_{tot} - C_2 - C_3 - 2C_4) / (Ni\ 2p_{3/2tot} + Co\ 2p_{3/2tot})$ was calculated and compared for each electrode material considered.

Looking at Table 2 it is possible to make some important observations regarding the surface chemical composition and properties of the GC/PVA/GO/Ni-Co electrodes:

a) The average composition of the electrodeposited Ni-Co particles, expressed as surface atomic ratio between the total areas of the Ni $2p_{3/2}$ and Co $2p_{3/2}$ XP signals, corrected by appropriate sensitivity [67,71], was about 0.19 ± 0.3 (i.e., $Ni_{16}Co_{84}$). This result is substantially in agreement with those obtained by electrochemical approach, where an "anomalous co-deposition" of Ni-Co species on the GC/PVA/GO substrate was hypothesized. In fact, a plating bath solution $[Ni^{2+}]:[Co^{2+}]$ of 0.33 produces a surface composition evaluated by XPS analysis of about 0.19 (i.e., ca - 74% expressed as atomic ratios).
b) The shape and BEs between the Ni $2p_{3/2}$ and Co $2p_{3/2}$ XP signals relevant at the Ni-Co material and individual Ni and Co deposits were virtually identical to each other. This result supports the view that the codeposited Ni-Co material preserves the specific chemical properties of the individual metals of which it is composed. In other words, no direct chemical interaction between Ni and Co deposited species can be hypothesized by XPS data.
c) The atomic ratios R(O/M), for each electrode material shows a values of about 2. This result supports the hypothesis that the surface of the electrode must contain mainly the $Ni(OOH)_2$, $Ni(OH)_2$, NiO_2, $Co(OOH)_2$, $Co(OH)_2$ and CoO_2, species.
d) The shape and the relative intensity of the peak contributes of the C 1s signal remain quite unchanged even after prolonged electrochemical treatment (cycling the potential between −0.1 e 0.7 V vs. SCE) in 0.1 M NaOH medium, indicating a good chemical stability of the PVA/GO electrode substrate.

Table 2
BEs (eV) of the XPS signals of GC/PVA/GO modified electrodes.

Electrode	C 1s	O 1s	Ni $2p_{3/2}$	Co $2p_{3/2}$	R(O/M)	Ni_xCo_y
GC/PVA/GO	284.6	530.5	–	–	–	–
	286.3	531.8				
	287.8	533.0				
GC/PVA/GO/Ni	284.6	530.9	856.2	–	2.2	–
	286.2	531.8	857.8			
	287.5	533.3				
	289.3					
GC/PVA/GO/Co	284.6	530.6	–	780.7	2.1	–
	286.2	531.6			782.2	
	287.7	533.0				
	289.2					
GC/PVA/GO/Ni-Co	284.6	531.2	856.4	781.5	1.9	$Ni_{18}Co_{82}$
	286.1	532.6	858.1		782.9	
	287.2	533.5				
	288.8					
GC/PVA/GO/Ni-Co*	284.6	530.2	856.5	781.1	2.2	$Ni_{14}Co_{86}$
	286.1	531.6	858.8	782.0		
	287.6	533.0				
	289.1					

GC/PVA/GO electrode obtained by casting 10 μL of the GO/PVA aqueous emulsion having a mass ratio of 5 onto GC surface and dried in an oven (50 °C for 20 min);
GC/PVA/GO/Ni electrode obtained as GC/PVA/GO and cycled between −0.5 V and 0.2 V vs. SCE (35 cycles) in 5.8 mM KCl solution plus 1.5 mM $Ni(NO_3)_2$;
GC/PVA/GO/Co electrode obtained as GC/PVA/GO and cycled between −0.5 V and 0.2 V vs. SCE (35 cycles) in 5.8 mM KCl solution plus 4.5 mM $Co(NO_3)_2$;
GC/PVA/GO/Ni-Co electrode obtained as GC/PVA/GO and cycled between −0.5 V and 0.2 V vs. SCE (35 cycles) in 5.8 mM KCl solution plus 1.5 mM $Ni(NO_3)_2$ and 4.5 mM $Co(NO_3)_2$;
GC/PVA/GO/Ni-Co* electrode obtained as GC/PVA/GO/Ni-Co and cycled in 0.1 M NaOH between 0.1 and 0.7 V vs. SCE, for 200 scans (50 mV s^{-1}).

4. Conclusions

In this study our interest was focused on the electrochemical, morphological and spectroscopic characterization of a composite GC/PVA/GO/Ni-Co electrode cycled in alkaline medium. An "anomalous co-deposition" of Ni-Co species on the GC/PVA/GO substrate was observed when the species were co-deposited simultaneously and a schematic mechanism of electrodeposition process was proposed. An average composition of the electrodeposited Ni-Co active material of $Ni_{16}Co_{84}$, was obtained. The beneficial effects of cobalt oxide species on the electrochemical redox behavior of the GC/PVA/GO/Ni-Co electrode have been highlighted and interpreted in light of current knowledge. The SEM analysis reveals that the GO particles appear as multi-layered agglomerated platelets dispersed in the PVA matrix, showing a disorder three-dimensional (3D) distribution with metal oxide particles with an average diameter comprised between 50 nm and 300 nm. XPS was used in order to evaluate the surface chemical composition of the GC/PVA/GO/Ni-Co electrode. An average atomic ratio R(O/M), very close to the value of 2, suggests that the $Ni(OOH)_2$, $Ni(OH)_2$, NiO_2, $Co(OOH)_2$, $Co(OH)_2$ and CoO_2 are the dominant species present on the GC/PVA/GO/Ni-Co electrode.

References

[1] J. Lipkowski, P.N. Ross (Eds.), Electrochemistry of Novel Materials: Frontiers of Electrochemistry, VCH Publishers, Inc., Weinheim, 1994.
[2] L. Bahadur, P. Srivastava, Sol. Energy Mater. Sol. Cells 79 (2003) 235–248.
[3] J. Su, X. Feng, J.D. Sloppy, L. Guo, C.A. Grimes, Nano Lett. 11 (2011) 203–208.
[4] M. Grätzel, Nature 414 (2011) 338–344.
[5] M.L. Zheludkevich, R. Serra, M.F. Montemor, M.G.S. Ferreira, Electrochem. Commun. 7 (2005) 836–840.
[6] X. Li, X. Nie, L. Wang, D.O. Northwood, Surf. Coat. Technol. 200 (2005) 1994–2000.
[7] C. Léger, C. Tessier, M. Ménétrier, C. Denage, C. Delmas, J. Electrochem. Soc. 146 (1999) 924–932.
[8] Z.-A. Hu, Y.-L. Xie, Y.-X. Wang, H.-Y. Wu, Y.-Y. Yang, Z.-Y. Zhang, Electrochim. Acta 54 (2009) 2737–2741.
[9] L. Xie, Z. Hu, C. Lv, G. Sun, J. Wang, Y. Li, H. He, J. Wang, K. Li, Electrochim. Acta 78 (2012) 205–211.
[10] M.F. Montemor, S. Eugénio, N. Tuyen, R.P. Silva, T.M. Silva, M.J. Carmezim, Nanostructured transition metal oxides produced by electrodeposition for application as redox electrodes for supercapacitors, in: M. Aliofkazraei, A.S.H. Makhlouf (Eds.), Handbook of Nanoelectrochemistry, Springer Int. Publ., Switzerland, 2016.
[11] A.C. Sonavane, A.I. Inamdar, P.S. Shinde, H.P. Deshmukl, P.S. Patil, J. Alloys Compd. 489 (2010) 667–673.
[12] R.J. Mortimer, D.R. Rosseinsky, P.M.S. Monk (Eds.), Electrochromic Materials and Devices, Wiley-VCH, Weinheim, 2015.
[13] W. Yan, D. Wang, G.G. Botte, Electrochim. Acta 61 (2012) 25–30.
[14] B. Habibi, E. Dadashpour, Int. J. Hydrog. Energy 38 (2013) 5425–5434.
[15] N. Sattarahmady, H. Heli, R.D. Vais, Biosens. Bioelectron. 48 (2013) 197–202.
[16] C.-W. Kung, Y.-H. Cheng, K.-C. Ho, Sensors Actuators B 204 (2014) 159–166.
[17] X. Tarrús, M. Montiel, E. Vallés, E. Gómez, Int. J. Hydrog. Energy 39 (2014) 6705–6713.
[18] T. Toda, H. Igarashi, H. Uchida, M. Watanabe, J. Electrochem. Soc. 146 (1999) 3750–3756.
[19] M.M. Jaksic, Int. J. Hydrog. Energy 26 (2001) 559–578.
[20] V.R. Stamenkovic, B.S. Mun, M. Arenz, K.J.J. Mayrhofer, C.A. Lucas, G. Wang, P.N. Ross, N.M. Markovic, Nat. Mater. 6 (2007) 241–247.
[21] S.K. Ghosh, M. Mandal, S. Kundu, S. Nath, T. Pal, Appl. Catal. A General 268 (2004) 61–66.
[22] H. Wu, D. Wexler, G. Wang, J. Alloys Compd. 488 (2009) 195–198.
[23] M. Asgari, M.G. Maragheh, R. Davarkhah, E. Lohrasbi, A.N. Golikand, Electrochim. Acta 22 (2012) 284–289.
[24] E.B. Castro, S.G. Real, L.F. Pinheiro Dick, Int. J. Hydrog. Energy 29 (2004) 255–261.
[25] F. Wolfart, A.L. Lorenzen, N. Nagata, M. Vidotti, Sensors Actuators B Chem. 186 (2013) 528–535.
[26] R.P. Silva, S. Eugénio, T.M. Silva, M.J. Carmezim, M.F. Montemor, J. Phys. Chem. C 116 (2012) 22425–22431.
[27] R.P. Silva, S. Eugénio, R. Duarte, T.M. Silva, M.J. Carmezim, M.F. Montemor, Electrochim. Acta 167 (2015) 13–19.
[28] J.-C. Chen, C.-T. Hsu, C.-C. Hu, J. Power Sources 253 (2014) 205–213.
[29] J. Zhang, F. Liu, J.P. Cheng, X.B. Zhang, Appl. Mater. Interfaces 7 (2015) 17630–17640.
[30] L. Gao, L. Wang, W. Zhang, X. Yang, Y. Ma, J. Shao, Electrochim. Acta 201 (2016) 260–267.
[31] L. Hu, L. Wu, M. Liao, X. Hu, X. Fang, Adv. Funct. Mater. 22 (2012) 998–1004.
[32] H. Wang, C.M.B. Holt, Z. Li, X. Tan, B.S. Amirkhiz, Z. Xu, B.C. Olsen, T. Sthephenson, D. Mitlin, Nano Res. 5 (9) (2012) 605–617.
[33] Y. Qian, S. Lu, F. Gao, J. Mater. Sci. 46 (2011) 3517–3522.
[34] T. Maiyalagan, X. Dong, P. Chen, X. Wang, J. Mater. Chem. 22 (2012) 5286–5290.
[35] Y. Tao, L. Ruiyi, L. Zaijun, Mater. Res. Bull. 51 (2014) 97–104.
[36] D. Chen, H. Feng, J. Li, Chem. Rev. 112 (2012) 6027–6053.
[37] A. García-Gómez, R.G. Duarte, S. Eugénio, T.M. Silva, M.J. Carmezim, M.F. Montemor, J. Electroanal. Chem. 755 (2015) 151–157.
[38] A. García-Gómez, S. Eugénio, R.G. Duarte, T.M. Silva, M.J. Carmezim, M.F. Montemor, Appl. Surf. Sci. 382 (2016) 34–40.
[39] X. Yang, Q. Yang, J. Xu, C.-S. Lee, J. Mater. Chem. 22 (2012) 8057–8062.
[40] Q. Xiao, X. Zhou, Electrochim. Acta 48 (2003) 575–580.
[41] K. Zhang, L.L. Zhang, X.S. Zhao, J. Wu, Chem. Mater. 22 (2010) 1392–1401.
[42] M.I. Baker, S.P. Walsh, Z. Schwartz, B.D. Boyan, J. Biomed. Mater. Res. B Appl. Biomater. 100B (2012) 1451–1457.
[43] A.A. Mohamad, N.S. Mohamad, M.Z.A. Yahya, R. Othman, S. Ramesh, Y. Alias, A.K. Arof, Solid State Ionics 156 (2003) 171–177.
[44] C. Bartholome, P. Miaudet, A. Derré, M. Maugey, O. Roubeau, C. Zakri, P. Poulin, Compos. Sci. Technol. 68 (2008) 2568–2573.
[45] C. Bao, Y. Guo, L. Song, Y. Hu, J. Mater. Chem. 21 (2011) 13942–13950.
[46] Z. Xu, C. Gao, ACS Nano 5 (2011) 2908–2915.
[47] D.W. Johnson, B.P. Dobson, K.S. Coleman, Curr. Opin. Colloid Interface Sci. 20 (2015) 367–382.
[48] J. Mc Breen, in: R.E. White, J.O. Bockris, B.E. Conway (Eds.), Modern Aspects of Electrochemistry, Plenum Press, New York, 1990.
[49] I.G. Casella, M.R. Guascito, M.G. Sannazzaro, J. Electroanal. Chem. 462 (1999) 202–210.
[50] M.C. Bernard, P. Bernard, M. Keddam, S. Senyarich, H. Takenouti, Electrochim. Acta 41 (1996) 91–93.
[51] A. Van der Ven, D. Morgan, Y.S. Meng, G. Ceder, J. Electrochem. Soc. 153 (2006) A210–A215.
[52] W.K. Behl, J.E. Toni, J. Electroanal. Chem. 31 (1971) 63–75.
[53] I.G. Casella, J. Electroanal. Chem. 520 (2002) 119–125.
[54] S. Palmas, F. Ferrara, A. Vacca, M. Mascia, A.M. Polcaro, Electrochim. Acta 53 (2007) 400–406.
[55] I.G. Casella, M. Contursi, J. Solid State Electrochem. 16 (2012) 3739–3746.
[56] C. Fan, D.L. Piron, Electrochim. Acta 41 (10) (1996) 1713–1719.
[57] E. Gómez, J. Ramirez, E. Vallés, J. Appl. Electrochem. 28 (1998) 71–79.
[58] R. Oriňáková, A. Turoňová, D. Kladeková, M. Gálová, R.M. Smith, J. Appl. Electrochem. 36 (2006) 957–972 and literature cited therein.
[59] M. Oshitani, H. Yufu, K. Takashima, S. Tsuji, Y. Mtsumaru, J. Electrochem. Soc. 136 (1989) 1590–1593.
[60] X.-Y. Wang, J.Y.Z. Zhou, J. Lin, H.-T. Yuan, D.-Y. Song, Y.-S. Zhang, L.-G. Zhu, Int. J. Hydrog. Energy 23 (1998) 873–878.
[61] R.S. Jayasharee, P.V. Kamath, J. Electrochem. Soc. 149 (2002) A761–A764.
[62] G. Wu, N. Li, De-R. Zhou, K. Mitsuo, Bo-Q. Xu, J. Solid State Chem. 177 (2004) 3682–3692.
[63] T.N. Ramesh, P.V. Kamath, Electrochim. Acta 53 (2008) 8324–8331.
[64] S.N. Begum, V.S. Muralidharan, C.A. Basha, J. Hydrogen Energy 34 (2009) 1548–1555.
[65] I.G. Casella, M. Gatta, J. Electrochem. Soc. 149 (2002) B465–B471.
[66] V. Gupta, S. Gupta, N. Miura, J. Power Sources 175 (2008) 680–685.
[67] C.D. Wagner, W.M. Riggs, L.E. Davis, J.F. Moulder, G.E. Mouilenberg, Handbook of X-ray Photoelectron Spectroscopy, Perkin-Elmer Corporation, Eden Prairie, Minnesota, 1978.
[68] E. Desimoni, I.G. Casella, A. Morone, A.M. Salvi, Surf. Interface Anal. 15 (1990) 627–634 and literature cited therein.
[69] A.P. Grosvenor, M.C. Biesinger, R.St.C. Smart, N.S. McIntyre, Surf. Sci. 600 (2006) 1771–1779.
[70] C.D. Wagner, L.E. Davis, M.V. Zeller, J.A. Taylor, R.M. Raymond, L.H. Gale, Surf. Interface Anal. 2 (1981) 211–225.
[71] I.G. Casella, M. Gatta, Anal. Chem. 72 (2002) 2969–2975.
[72] I.G. Casella, M.R. Guascito, J. Electroanal. Chem. 476 (1999) 54–63.
[73] A. Foelske, H.-H. Strehblow, Surf. Interface Anal. 34 (2002) 125–129.